REPORT DOCUMENTATION PAGE

Form Approved
OMB No. 0704-0188

1. REPORT DATE *(DD-MM-YYYY)* 28 May 2003	**2. REPORT TYPE** Technical Paper	**3. DATES COVERED** *(From - To)*
4. TITLE AND SUBTITLE **Preliminary Experiments for Evaluating 3-D Effects on Cracks in Frozen Stress Models**		**5a. CONTRACT NUMBER**
		5b. GRANT NUMBER
		5c. PROGRAM ELEMENT NUMBER
6. AUTHOR(S) C.W. Smith[1], J.D. Hansen[1], C.T. Liu[2]		**5d. PROJECT NUMBER** 2302
		5e. TASK NUMBER 0378
		5f. WORK UNIT NUMBER
7. PERFORMING ORGANIZATION NAME(S) AND ADDRESS(ES) [1]Department of Engineering Science and Mechanics Polytechnic Institute and State University Blacksburg, VA 24061	[2]Air Force Research Laboratory (AFMC) AFRL/PRSM 10 E. Saturn Blvd. Edwards AFB CA 93524-7680	**8. PERFORMING ORGANIZATION REPORT NUMBER** AFRL-PR-ED-TP-2003-141
9. SPONSORING / MONITORING AGENCY NAME(S) AND ADDRESS(ES) Air Force Research Laboratory (AFMC) AFRL/PRS 5 Pollux Drive Edwards AFB CA 93524-7048		**10. SPONSOR/MONITOR'S ACRONYM(S)**
		11. SPONSOR/MONITOR'S NUMBER(S) AFRL-PR-ED-TP-2003-141

12. DISTRIBUTION / AVAILABILITY STATEMENT

Approved for public release; distribution unlimited.

13. SUPPLEMENTARY NOTES

14. ABSTRACT

20030801 110

15. SUBJECT TERMS

16. SECURITY CLASSIFICATION OF:			**17. LIMITATION OF ABSTRACT**	**18. NUMBER OF PAGES**	**19a. NAME OF RESPONSIBLE PERSON** Sheila Benner
a. REPORT Unclassified	**b. ABSTRACT** Unclassified	**c. THIS PAGE** Unclassified	A		**19b. TELEPHONE NUMBER** *(include area code)* (661) 275-5693

Standard Form 298 (Rev. 8-98)
Prescribed by ANSI Std. 239.18

FILE

MEMORANDUM FOR PRS (In-House Publication)

FROM: PROI (STINFO)

28 May 2003

Lim
Slkav

SUBJECT: Authorization for Release of Technical Information, Control Number: **AFRL-PR-ED-TP-2003-141**
C.W. Smith (VA Poly Inst); J.D. Hansen (VA Poly Inst); C.T. Liu (AFRL/PRSM), "Preliminary Experiments for Evaluating 3-D Effects on Cracks in Frozen Stress Models"

ASME Int'l Mechanical Engineering Congress & Exhibition
(Washington, D.C., 16-21 November 2003) (Deadline = 20 June 2003)

(Statement A)

Proceedings of IMECE 2003
ASME International Mechanical Engineering Congress & Exposition
November 16-21, 2003, Washington, DC

IMECE2003-43489

PRELIMINARY EXPERIMENTS FOR EVALUATING 3-D EFFECTS ON CRACKS IN FROZEN STRESS MODELS

C. W. Smith[1], J. D. Hansen[1] and C. T. Liu[2]

[1] Department of Engineering Science and Mechanics
Virginia Polytechnic Institute and State University
Blacksburg, Virginia 24061

[2] Air Force Research Laboratory, PRSM
10 E. Saturn Blvd.
Edwards AFB, California 93524-7680

ABSTRACT

Information gleaned from applying the frozen stress photoelastic method to cracks emanating from critical locations around the fin tips in models of solid rocket motors is reviewed and assessed together with new experimental results. The studies are the initial part of a program developed to contribute background data for consideration in modifying current motor grain design rationale.

INTRODUCTION

Computational analysis and two dimensional tensile tests on single motor grain fins suggest that cracks in fin tips are most likely to originate at the point of coalescence of the fin tip end radius with a small radius connecting the fin tip end radius with the side of the fin. We call such cracks off-axis cracks. Designers of motor grain geometry, however, assume the critical crack to originate on the fin axis as a Class 1 crack. Frozen stress experiments show that the former type of crack (i.e. off-axis) is initially a Class 2 crack under mixed mode load and must turn to eliminate the shear modes before becoming a Class 1 crack. Cotterell, (1995) in differentiating between Class 1 and Class 2 cracks, noted that all Class 2 cracks become Class 1 cracks if allowed sufficient growth. In the present discussion, we shall find that Class 2 cracks are those sustaining mixed mode loads and will reorient their growth paths to ~~eliminate the shear modes in order to attain Class 1~~ status, which exhibit no shear modes in our current test program.

THE EXPERIMENTS

Recent frozen stress experiments have been conducted by Smith, Constantinescu and Liu (2002) on off-axis cracks emanating from the coalescence of the large fin tip radius R11 (Fig. 1), and the small radius R1.3 (Fig. 1) which also coalesces with the side of the fin. Starter cracks were initiated in two ways:

i. Normal to the fin surface

ii. Parallel to the fin axis

Both cracks were inserted by striking a sharp blade held against the fin surface at the above noted critical point. The starter cracks emanated from the tip of the blade into the material. The test models were then heated above critical temperature (Appendix A) and then internal pressure was applied in order to grow the crack to its desired size after which the pressure was reduced to stop the crack growth and the models were slowly cooled to room temperature and the load removed. Thin slices were then removed mutually orthogonal to each flaw border and its surface and analyzed photoelastically as two dimensional models but containing the three dimensional effect. The photoelastic data were then converted into stress intensity factors (SIF^s) using a two parameter algorithm (Smith and Kobayashi, 1993). The Mode I and Mode II algorithms for these calculations are given in Appendix B.

For the off-axis cracks normal to the fin surface, Fig. 2 shows two such cracks which can be regarded as the same crack at different stages of its growth. During the first stage (Model 1, Fig. 2a) the crack turns all along its border under the action of both Modes I and II everywhere except at the fin surface where only Mode I exists. Section SS suggests that the starter crack was planar until turning began. Model 2, (Fig. 2b) shows another crack which has experienced additional growth. After turning under Modes I and II, this crack exhibits river markings indicating Mode III as well as I and II until it completes its turning and becomes parallel to the fin axis. No calculations were made near the river markings because small deformation theory may have been exceeded there. At the stage of growth shown in Model 2 (Fig. 2b) only pure Mode I exists all along the crack border and it has become a Class 1 crack.

For off-axis cracks parallel to the fin axis, a small damage zone occurred when the crack entered the material and it then emerged in a direction approximately parallel to the fin axis. (Section SS of Model 3, Fig. 3). The crack shown in Fig. 3 had also achieved Class 1 status.

Although ample evidence appears in Fig. 3 of the presence of Mode II turning and Mode III river markings, the effects here produce what appears as only negligible turning as shown by Section SS.

It is this type of crack which we wish to make comparisons with symmetric cracks on the fin axis, as shown on Fig. 1. For this purpose, a series of tests on models containing a single symmetric crack as located in Fig. 1 were tested using the same procedures as were described above. To date two such tests have been completed (Models 4 and 5). One such crack (Model 4) is shown in Fig. 4, and is a planar, Class 1 semi-elliptic crack with pure Mode I all around the crack border.

RESULTS

Test data and results, including those for Models 1 and 2 discussed above are presented in Table 1. Models 3 and 4 are similar in most respects except that Model 3 was an off-axis crack with blade parallel to the fin axis while Model 4 was a symmetric crack on the fin axis. Results from a second, deeper symmetric crack (Model 5) can be compared to results from the average of two off-axis cracks with blades parallel to the fin axis which were in the same test specimen (Model 6) but were separated by an uncracked fin as per Fig. 1. Finally, Fig. 5 shows the path of the mid point of an off-axis crack (Model 7) with blade parallel to the fin axis which grew to and penetrated the outer boundary of the model. This suggests that, once the off-axis cracks have cleared a region of about half the fin width around the crack tip, they will follow paths parallel to the symmetric cracks to the model boundary. It is also noted that the average a/c for two symmetric cracks which penetrated the boundary in other tests was 0.79 as compared with 0.77 for Model 7.

Table 1: Table 1 – Data and Results

Loads[1]	Crack size[2] (dimensions in mm)	F_i[3]	Notations
p_{max} = 0.049 MPa p_{sf} = 0.035 MPa	**Model 1** off-axis normal to surface a = 8.71 Δa = 2.18 c = 11.15 Δc = 3.02 a/c = 0.78 a/t = 0.23	$F_1 = 2.09$ $F_2 = 0.53$	1. p_{max} = internal pressure to grow crack p_{sf} = stress freezing pressure
p_{max} = 0.103 MPa p_{sf} = 0.049 MPa	**Model 2** off-axis normal to surface a = 12.50 Δa = 3.40 c = 21.10 Δc = 10.40 a/c = 0.59 a/t = 0.34	2.19 0	2. a = crack depth; Δa = crack growth c = half length of crack in fin tip surface Δc = half crack growth in fin tip surface
3. p_{max} = 0.103 MPa p_{sf}= 0.049 MPa	**Model 3** off-axis parallel to fin axis a = 7.9 Δa = 2.80 c = 13.35 Δc = 7.75 a/c = 8.59 a/t = 0.21	2.12 0	3. $F_i = K\sqrt{Q}/p_{sf}\sqrt{\pi a}$ i = 1, 2, at maximum depth $\sqrt{Q}$ = approximation of elliptic integral second kind
p_{max} = 0.121 MPa p_{sf} = 0.041 MPa	**Model 4** symmetric, on fin axis a = 8.13 Δa = 2.80 c = 12.58 Δc = 6.10 a/c = 0.65 a/t = 0.22	2.21 0	$Q = 1 + 1.464(\frac{a}{c})^{1.65}$ $\frac{a}{c} \leq 1$
p_{max} = 0.129 MPa p_{sf} = 0.046 MPa	**Model 5** symmetric on fin axis a = 14.6 Δa = 5.1 c = 23.0 Δc = 13.0 a/c = 0.64 a/t = 0.39	1.71 0	All flaws were characterized as semi-elliptic flaws of depth a and length 2c. However, off-axis cracks were neither perfectly semi-elliptic nor planar.
p_{max} = 0.103 MPa p_{sf} = .049 MPa	**Model 6** off-axis parallel to fin axis a = 14.75 Δa = 7.03 c = 22.55 Δc = 13.87 a/c = 0.65 a/t = 0.40	1.73 0	
p_{max} = 0.110 MPa p_{sf} = 0.049 MPa	**Model 7** off-axis parallel to fin axis a = 37.08 Δa = 30.9 c = 48.0 Δ_c = 41.65 a/c = 0.77 a/t = 1.00	–	

DISCUSSION

On the basis of the results to date, there appears to be a substantial similarity between the off-axis and the symmetric cracks, both with respect to normalized SIF^s (Fi) and also crack paths, particularly when the former achieves Class 1 status. However, there is some initial reorientation of the off-axis cracks to eliminate shear modes before achieving Class 1 status, after which they travel parallel to the fin axis. Once this reorientation occurs, it may be unimportant to differentiate betwen the two types of cracks. However, for the full growth period, one must recognize that the symmetric crack exhibits Class 1 status from its inception.

Experiments on deeper symmetric cracks are continuing and will be complemented with equal depth cracks which run all the way to the ends of the motor grain models. Final results will be used to assess current design rationale which is based upon the latter type of crack. These preliminary results however, suggest that part through cracks break through to the outer circumference of the model before running the length of the cylindrical model and might be a candidate for replacing the through crack used in current design.

ACKNOWLEDGEMENTS

The authors wish to gratefully acknowledge the support of the Air Force Research Laboratory through Sparta Inc. Sub-Contract 01655-Mod I and the staff and facilities of the VPI&SU, Department of Engineering Science and Mechanics.

REFERENCES

1 Cotterell, B., "On Brittle Fracture Paths," *International Journal of Fracture Mechanics*, Vol. 1, pp. 96-103, 1965.

2 Smith, C. W. and Kobayashi, A. S., " Experimental Fracture Mechanics," *Handbook on Experimental Mechanics*, (2nd Revised Ed.) Chapter 20, pp. 905-968, 1993.

3 Smith, C. W., Constantinescu, D. M. and Liu, C. T., " Stress Intensity Factors and Crack Paths for Cracks in Photoelastic Motor Grain Models," *Proceeedings of ASME International Mechanical Engineering Conference and Exposition IMECE 2002-32078*, pp. 1-8, 2002.

APPENDIX A- Frozen Stress Photoelasticity

When a transparent model is placed in a circularly polarized monochromatic light field and loaded, dark fringes will appear which are proportional to the applied load. These fringes are called stress fringes or isochromatics, and the magnitude of the maximum in-plane shear stress is a constant along a given fringe.

Some transparent materials exhibit mechanical diphase characteristics above a certain temperature, called the critical temperature (T_c). The material, while still perfectly elastic will exhibit a fringe sensitivity of about twenty times the value obtained at room temperature, and its modulus of elasticity will be reduced to about one six-hundredth of its room temperature value. By raising the model temperature above T_c, loading, and then cooling slowly to room temperature, the stress fringes associated with T_c will be retained when the material is returned to room temperature. Since the material is so much more sensitive to fringe generation above T_c than at room temperature, fringe recovery at room temperature upon unloading is negligible. The model may then be sliced without disturbing the "frozen in" fringe pattern and analyzed as a two-dimensional model but containing the three-dimensional effects. In the use of the method to make measurements near crack tips, due to the need to reduce loads above critical temperature to preclude large local deformations, and the use of thin slices, few stress fringes are available by standard procedures. To overcome this obstacle, a refined polariscope is employed to allow the tandem use of the Post and Tardy methods to increase the number of fringes available locally.

In fringe photographs, integral fringes are dark in a dark field and bright in a bright field.

Appendix B

Mode I Algorithm

Beginning with the Griffith-Irwin Equations, we may write, for Mode I, for the homogeneous case,

$$\sigma_{ij} = \frac{K_1}{(2\pi\tau)^{\frac{1}{2}}} f_{ij}(\theta) + \sigma_{ij}^{\circ} \qquad (i,j = n,z) \qquad (1)$$

where:

σ_{ij} are components of stress

K_1 is SIF

r, θ are measured from crack tip (Fig. B-1)

σ_{ij}° are non-singular stress components

Then, along $\theta = \pi/2$, after truncating σ_{ij}

$$\tau_{nz}^{max} = \frac{K_1}{(8\pi\tau)^{\frac{1}{2}}} + \tau^{\circ} = \frac{K_{AP}}{(8\pi\tau)^{\frac{1}{2}}} \qquad (2)$$

where:

$\tau^{\circ} = f(\sigma_{ij}^{\circ})$ and is constant over the data range

K_{AP} = apparent SIF

τ_{nz}^{max} = maximum shear stress in nz plane

Normalizing with respect to $\bar{\sigma}$,

$$\therefore \frac{K_{AP}}{\bar{\sigma}(\pi a)^{\frac{1}{2}}} = \frac{K_1}{\bar{\sigma}(\pi a)^{\frac{1}{2}}} + \frac{\sqrt{8}\tau^{\circ}}{\bar{\sigma}} \left(\frac{r}{a}\right)^{\frac{1}{2}} \qquad (3)$$

where (Fig. B-1) a = crack length, and $\bar{\sigma}$ = remote normal stress

i.e $\frac{K_{AP}}{\bar{\sigma}(\pi a)^{\frac{1}{2}}}$ vs. $\sqrt{\frac{r}{a}}$ is linear.

From the Stress-Optic Law, $\tau_{nz}^{max} = nf/2t$ where,

n = stress fringe order,

f = material fringe value, and

t = specimen (or slice) thickness

then from Eq. 2

$$K_{AP} = \tau_{nz}^{max}(8\pi r)^{\frac{1}{2}} = \frac{nf}{2t}(8\pi r)^{\frac{1}{2}}$$

where K_{AP} (through a measure of n) and r become the measured quantities from the stress fringe pattern at different points in the pattern.

In the present study, instead of normalizing K with respect to $\bar{\sigma}(\pi a)^{1/2}$, we have selected $p_{sf}\sqrt{\pi a/Q}$ as the normalizing factor where $\sqrt{Q}$ is an elliptic integral of the second kind approximated here, as shown in Table I. An example of the determination of F_1 in Table I from test data is given in Fig. B-2.

Mixed Mode Algorithm

The mixed mode algorithm was developed (see Fig. B-3) by requiring that:

$$\lim_{\substack{r_m \to 0 \\ \theta_m \to \theta_m^{\circ}}} \left\{ (8\pi r_m)^{1/2} \frac{\delta(\tau)_{nz}^{max}}{\delta\theta} (K_1, K_2, r_m, \theta_m, \tau_{ij}) \right\} = 0 \qquad (4)$$

which leads to:

$$\left(\frac{K_2}{K_1}\right)^2 - \frac{4}{3}\left(\frac{K_2}{K_1}\right) cot\ 2\theta_m^{\circ} - \frac{1}{3} = 0 \qquad (5)$$

By measuring θ_m° which is approximately in the direction of the applied load, K_2/K_1 can be determined.

Then writing the stress optic law as:

$$\tau_{nz}^{max} = \frac{fn}{2t} = \frac{K_{AP}^*}{(8\pi r)^{\frac{1}{2}}}$$

where K_{ap}^* is the mixed mode SIF, one may plot $\frac{K_{AP}^*}{\bar{\sigma}(\pi a)^{\frac{1}{2}}}$ vs. $\sqrt{r/a}$ as before, locate a linear zone and extrapolate to $r = 0$ to obtain K^*. Knowing, K^*, K_2/K_1 and θ_m°, values of K_1 and K_2 may be determined since

$$K^* = [(K_1 sin\theta_m^{\circ} + 2K_2 cos\theta_m^{0})^2 + (K_2 sin\theta_m^{\circ})^2]^{\frac{1}{2}} \qquad (6)$$

Knowing K^* and θ_m°, K_1 & K_2 can be determined from Eqs. 5 and 6. Details are found in Smith and Kobayashi (1993).

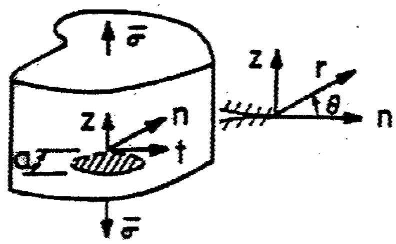

Fig. B-1 Near Tip Notation for Mode I.

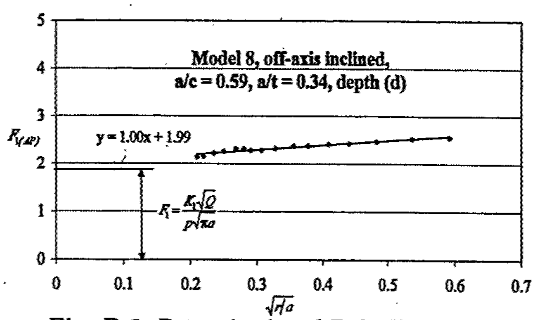

Fig. B-2: Determination of F_1 for Test Data.

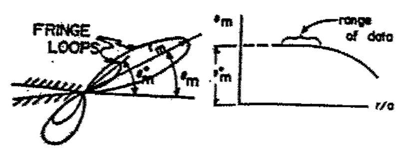

Fig. B-3: Determination of θ_m^o for Mixed Mode

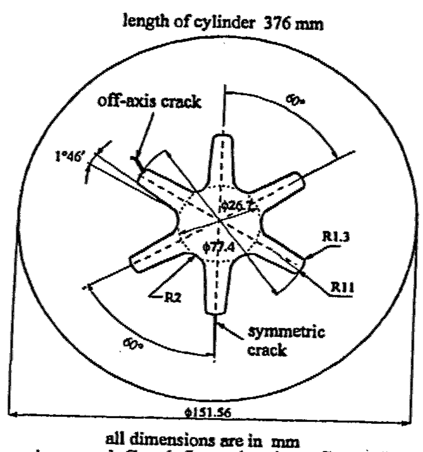

Figure 1: Dimensions and Crack Location in a Cross-Section of a Model

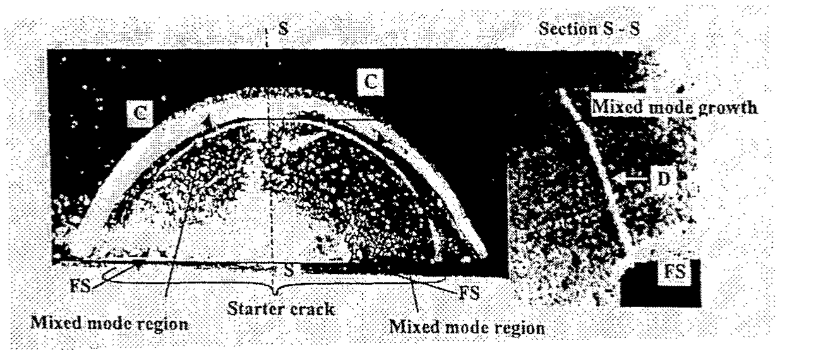

Fig. 2a Model 1 Off-Axis Inclined Crack Showing Starter Crack and Final Crack Front

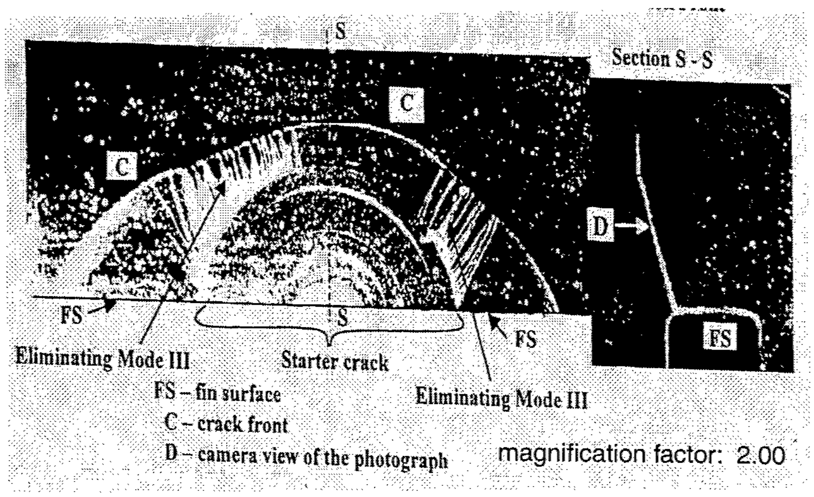

Fig. 2b Model 2 Off-Axis Inclined Crack Showing Starter Cracks and Final Mode I Crack Front

Figure 2: Typical Off-Axis Inclined Cracks (Blade Held Normal to Fin Surface)

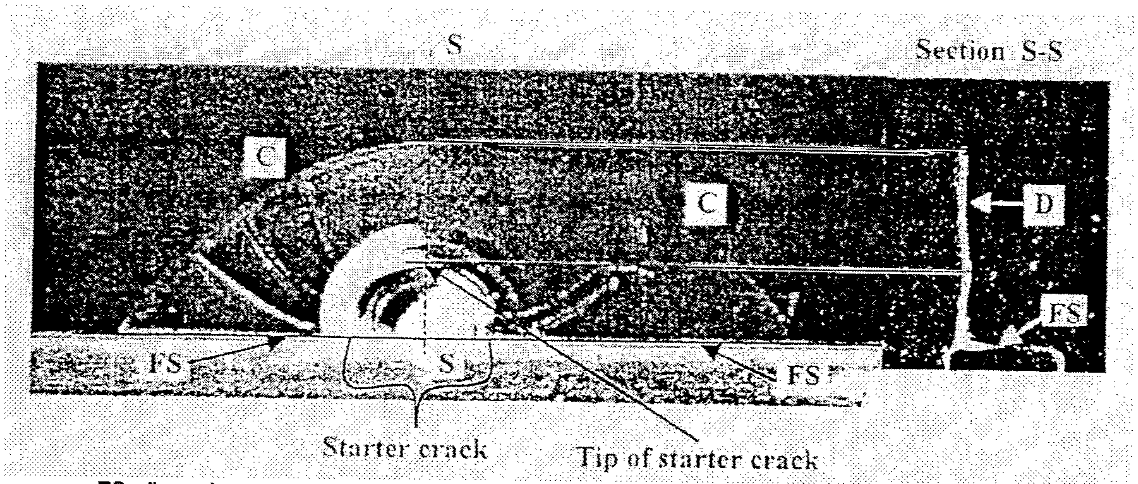

FS - fin surface
C - crack front
D - camera view of the photograph

magnification factor: 1.73

Figure 3: Typical Off-Axis Crack (Blade Held Parallel to Fin Axis) Model 3

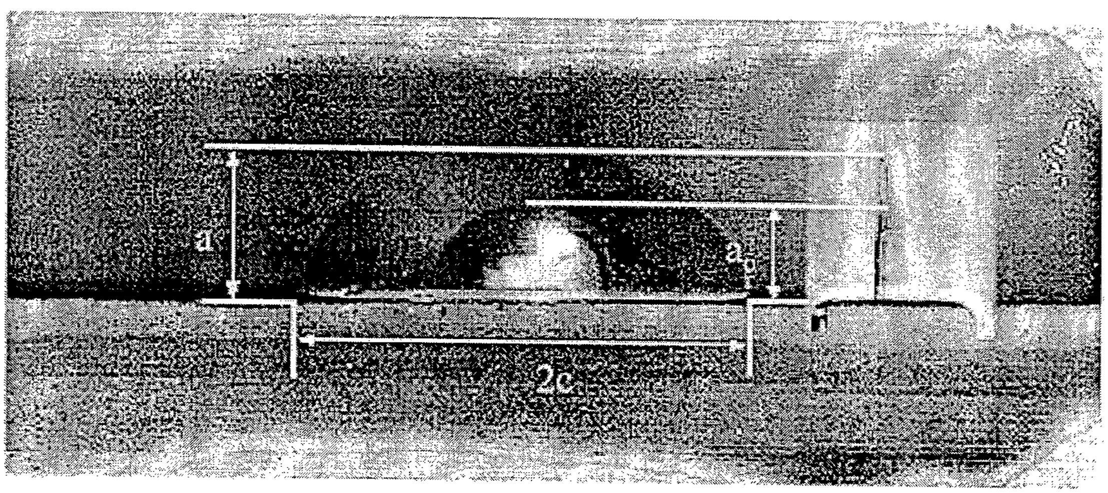

M.F 2.52

Figure 4: Symmetric Crack Originating on Fin Axis (Model 4).

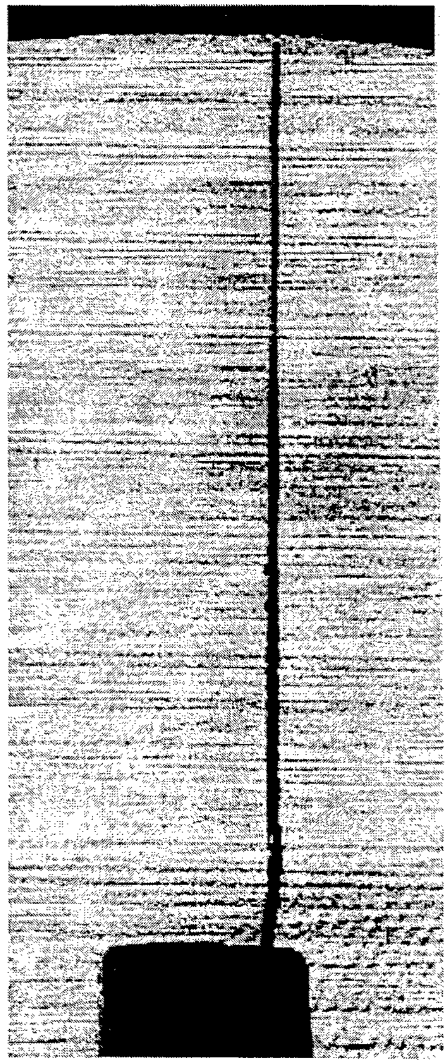

Figure 5: Off-Axis Crack Path (Blade Held Parallel to Fin Axis). Model 7.